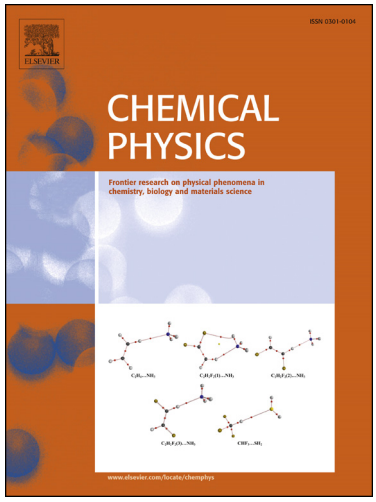

Experimental and Theoretical Studies of the Second- and Third-Order NLO Properties of a semi-organic compound: 6-Aminoquinolinium Iodide Monohydrate

Pedro S. Pereira Silva, Hasnaa El Ouazzani, Mindaugas Pranaitis, Manuela Ramos Silva, Cláudia T. Arranja, Abilio J.F.N. Sobral, Bouchta Sahraoui, José A. Paixão

PII: S0301-0104(13)00406-0
DOI: http://dx.doi.org/10.1016/j.chemphys.2013.11.001
Reference: CHEMPH 8986

To appear in: *Chemical Physics*

Received Date: 31 May 2013
Accepted Date: 3 November 2013

Please cite this article as: P.S. Pereira Silva, H.E. Ouazzani, M. Pranaitis, M.R. Silva, C.T. Arranja, A.J.F. Sobral, B. Sahraoui, J.A. Paixão, Experimental and Theoretical Studies of the Second- and Third-Order NLO Properties of a semi-organic compound: 6-Aminoquinolinium Iodide Monohydrate, *Chemical Physics* (2013), doi: http://dx.doi.org/10.1016/j.chemphys.2013.11.001

Experimental and Theoretical Studies of the Second- and Third-Order NLO Properties of a semi-organic compound: 6-Aminoquinolinium Iodide Monohydrate

Pedro S. Pereira Silva[a,*], Hasnaa El Ouazzani[b], Mindaugas Pranaitis[b], Manuela Ramos Silva[a], Cláudia T. Arranja[c], Abilio J. F. N. Sobral[c], Bouchta Sahraoui[b], José A. Paixão[a]

[a] *CEMDRX, Physics Department, University of Coimbra, P-3004-516 Coimbra, Portugal*
[b] *Institut des Sciences et Technologies Moléculaires d'Angers, MOLTECH ANJOU, CNRS UMR 6200, Université d'Angers, 2 Bd Lavoisier, 49045 Angers Cedex, France*
[c] *Department of Chemistry, University of Coimbra, P-3004-516 Coimbra, Portugal*

Abstract

A new semi-organic compound, 6-aminoquinolinium iodide monohydrate (**I**), has been synthesized and characterized by single crystal X-ray diffraction, UV-Vis absorption and fluorescence spectroscopy and nonlinear optical (NLO) measurements. The second- and third-order NLO responses were investigated with the second- and third-harmonic Maker fringes techniques, carried out on thin films at a fundamental wavelength of 1064 nm. From the molecular structure, the molecular hyperpolarizability tensors were determined with density functional theory and second-order Møller-Plesset perturbation method. The second- and third-order susceptibility tensors of the reported crystal were evaluated using the oriented gas model with the Lorenz-Lorentz and the Wortmann-Bishop local-field corrections. The calculations using the Wortmann-Bishop local-field were able to reproduce the correct order of magnitude of the experimental third-order susceptibilities. The value of $\chi^{(3)}$ obtained by summing the effective third-order polarizability calculated for the asymmetric unit surrounded by ESP-derived charges have also the same order of magnitude of the experimental.

Keywords: Single crystal X-ray diffraction, Nonlinear optics, Maker

*Corresponding author. E-mail address: psidonio@pollux.fis.uc.pt (Pedro S. Pereira Silva)

fringes, SHG, THG, *Ab initio* calculations, DFT, MP2, Local field corrections, ESP-derived charges

1. Introduction

The majority of the early nonlinear optical (NLO) materials were based on inorganic crystals but in the last three decades the focus has shifted toward organic compounds due to their promising potential applications in optical signal processing [1, 2]. Some of the advantages offered by the organic materials are the high values of electronic susceptibility [3, 4], fast response times and much greater versatility in molecular design, compared with their inorganic counterparts. However, purely organic compounds lack mechanical strength for practical uses and it is difficult to grow single crystals of sufficient quality. For this reason the crystal engineering strategy of combining organic and inorganic moieties was proposed with the objective of building more cohesive crystalline structures [5]. Several examples of hybrid organic-inorganic crystals have emerged as good candidates for NLO materials [6, 7, 8, 9]. These systems exhibit high nonlinear optical efficiency in the visible region and good thermal and mechanical stability compared with those of purely organic crystals. Besides these advantages, it was demonstrated by Evans *et al.*[10] that the proton transfer occurring in acid/base reactions, often used to synthesize these hybrid materials, can enhance the hyperpolarizabilities of the chromophores.

Salts of quinoline[11] and quinoline derivatives[12] have shown interesting NLO properties and that prompted our interest in probing salts of 6-aminoquinoline. We present here the crystal structure and the results of spectroscopic and nonlinear optical measurements for a a novel semi-organic compound, 6-aminoquinolinium iodide monohydrate. In this study, the second and third order nonlinear susceptibilities, $\chi^{(2)}$ and $\chi^{(3)}$, respectively, are calculated with the oriented gas model.

Knowing the crystal structure of a compound, its macroscopic nonlinear optical properties can be estimated by assuming the additivity of the molecular hyperpolarizabilities, according to the oriented gas model, first employed by Chemla *et al.*[13]. In this model, the macroscopic crystal susceptibilities are obtained by performing a tensor sum of the microscopic hyperpolarizabilities of the unit cell and the effects of the surrounding medium are described by appropriate local field factors.

In the present work, the nonlinear optical properties of the microscopic units are calculated with density functional theory (DFT), using several functionals, and with the second-order Møller-Plesset perturbation method (MP2). The DFT methods are less computationally demanding than MP2 and present a compromise between computational cost and accuracy of the results however, it is well-known that DFT overestimates NLO properties [14, 15, 16]. One way of correcting this problem is the use of functionals with a high percentage of HF-exchange [14, 16, 17]. For the macroscopic properties we use two different local field corrections: the anisotropic Lorenz-Lorentz spherical cavity local field factors and the local field factors deduced by Wortmann and Bishop (W-B)[18] from an extension of the Onsager's reaction field model [19]. However, it must be pointed out that the intermolecular interactions in crystals, overlooked by the gas oriented model, may have an enhancing or diminishing effect on hyperpolarizability [20, 21], so as an alternative to the calculations with the local field corrections, we have also calculated the molecular hyperpolarizabilities using ElectroStatic Potential (ESP) charges to describe the medium around the asymmetric unit. Very recently, it was developed one method, the finite field Berry phase approach [22], that makes the approximations underlying the oriented gas model unnecessary and allows one to predict nonlinear susceptibilities directly.

In this work, the performance of the calculation methods is assessed by comparing the calculated values of the susceptibilities with the experimental ones.

The paper is organized as follows: in section two we describe the experimental methods used in this work. Section three comprises the theoretical methodologies implemented. In section four the results (crystal structure and optical properties) are discussed and the conclusions are presented in section five.

2. Experimental Section

2.1. Synthesis and Sample Preparation

Hydroiodic acid (Fluka, 55−58%, 1mmol) was added to 6-aminoquinoline (TCI, > 97%, 1mmol) in a water solution (150 mL). The solution was stirred for 30 min at 40°C and left to evaporate under ambient conditions. After approximately 1 month, yellow and transparent single crystals with thin plate habit were deposited.

We prepared thin films for the SHG and THG measurements depositing small drops of a 5 mM water solution of the title compound on top of glass (Chevallier S.A. glasses) and letting the solution evaporate slowly in a heating plate at 70 °C. The thickness of the films used in the Maker fringes measurements was 800 nm approximately .

2.2. Single Crystal X-ray Diffraction

The diffraction measurements for 6-aminoquinolinium iodide monohydrate were carried out with a single crystal on a Bruker APEX II diffractometer using Mo Kα radiation [23]. Data reduction was performed with SMART and SAINT software [23]. Lorenz and polarization corrections were applied. A multi-scan absorption correction was applied using SADABS [24]. The structure was solved by direct methods using SHELXS-97 program [25], and refined on F^2s by full-matrix least-squares with SHELXL-97 program [25]. The anisotropic displacement parameters for non-hydrogen atoms were applied. The hydrogen atoms were placed at calculated positions and refined with isotropic parameters as riding atoms, except the hydrogen atoms of the water molecule that were located in a difference Fourier synthesis at an intermediate stage of the refinement and then allowed to refine as riding atoms. The crystal data and details concerning data collection and structure refinement are given in Table 1.

2.3. UV-vis Absorption and Fluorescence Spectra

Absorption spectra were recorded in a Jasco V-530 double-beam UV/Vis spectrophotometer in quartz cells with 1 cm path length using ultra-pure water as solvent and reference. Steady-state fluorescence studies were carried out using a Jobin-Yvon SPEX Fluorolog 3-22 spectrometer. Fluorescence spectrum was taken with excitation at 377 nm and was automatically corrected for the wavelength response of the system.

2.4. Nonlinear Optical Techniques

2.4.1. Z-Scan

The nonlinear absorption of the title compound was investigated with "open-aperture" Z-scan measurements employing 532 nm, 35 ps laser pulses, following the procedure described elsewhere [26, 27]. Briefly, in the Z-scan technique, the transmittance of a sample is measured as it moves along the propagation direction of a focused Gaussian laser beam, therefore experiencing different intensity at each position. By fitting the experimental data

Table 1: Crystal data and structure refinement of 6-aminoquinolinium iodide monohydrate.

Chemical formula	$C_9H_{11}IN_2O$
Formula weight	290.10
Temperature (K)	293(2)
Wavelength (Å)	0.71073
Crystal system	Orthorhombic
Space group	$P2_12_12_1$
a (Å)	6.5944(4)
b (Å)	10.4425(6)
c (Å)	15.8413(9)
$\alpha(^\circ)$	90
$\beta(^\circ)$	90
$\gamma(^\circ)$	90
Volume (Å^3)	1090.86(11)
Z	4
Calc. dens.(g/cm^3)	1.766
Abs. coef. (mm^{-1})	2.901
$F(000)$	560
Crystal size (mm)	0.36×0.35×0.11
data collection range	3.23-29.07°
Index ranges: h	-8, 9
k	-14, 14
l	-21, 20
Reflections:	
collected	12229
unique	2894
R(int)	0.0323
Completeness (θ=25.00°)	99.8%
Refinement method	Full-matrix least-squares on F^2
Data/restraints/ parameters	2894/0/118
F^2 Goodness-of-fit	1.016
R indices:	
final [$I > 2\sigma(I)$]	0.0259
wR_2	0.0643
all data	0.0362
wR_2	0.0703
Largest diff. peak and hole (eÅ^{-3})	0.343 -0.686

according to equations which can be found in the literature [26, 27], the nonlinear absorption parameter, β, the Im $\chi^{(3)}$ and Im γ values can be obtained.

Before the measurements, we performed a calibration of the nonlinear absorption setup using samples of C60 fullerene, which is a well known optical limiter. Then, "open-aperture" Z-scan measurements have been done for several concentrations of the title compound and for various incident laser intensities.

2.4.2. SHG and THG Measurements

The second and third order nonlinear optical responses of thin films were studied with the SHG and THG Maker fringes experimental techniques in transmission, using a 30 ps diode pumped passively mode-locked Nd:YVO_4 laser, with a repetition rate of 10 Hz. The intensity and the polarization of the fundamental beam (1064 nm) exciting the sample were precisely adjusted by a half wave plate and a polarizer. The intensity at the input face of the sample was assumed to have a Gaussian temporal and spatial profile. The laser beam was focused by a lens (f = 250 mm) on the sample, which had been positioned near the focal plane. The films were mounted on a motorized rotational stage allowing the variation of the incident angle with a resolution of 0.5 ° around the normal of the incident beam. After passing through a KG3 filter, which cut out the fundamental beam, and interference filters (532 nm for SHG and 355 nm for THG) to preserve only the SHG/THG signal, the latter was detected with a photomultiplier (PMT), which was connected with a boxcar averager and a computer. Neutral density (ND) filters have been always positioned before the PMT to avoid saturation. The so-called Maker fringes [28] were finally obtained by rotating the sample in the range $\pm 60°$ to the normal. Maker fringes measurements have been done for both s and p polarizations.

The data analysis of the second order susceptibilities was performed by comparison with the SHG intensity of a standard 0.5 mm thick Y-cut quartz crystal plate. The simplified model of Lee *et al.* was used [29]

$$\frac{\chi^{(2)}}{\chi_q^{(2)}} = \frac{2}{\pi}\frac{l_{c,q}}{d}\sqrt{\frac{I^{2\omega}}{I_q^{2\omega}}} \tag{1}$$

where $\chi^{(2)}$ and $\chi_q^{(2)}$ denote the second-order nonlinear susceptibilities of the studied material and quartz, respectively, $I^{2\omega}$ and $I_q^{2\omega}$ are the second har-

monic intensities of the material studied and quartz, respectively, d is the film thickness and $l_{c,q}$ is the coherence length of quartz (20.5 μm [30]).

For THG data analysis we used the model of Kubodera and Kobayashi [31]. This model compares directly the maximal amplitudes of third harmonic light intensity of the studied material with those of a 1 mm silica slab as reference. For a weak absorption, the relation used to determine the magnitude of $\chi^{(3)}$ is given by

$$\frac{\chi^{(3)}}{\chi^{(3)}_S} = \frac{2}{\pi}\frac{L_{c,S}}{d}\sqrt{\frac{I^{3\omega}}{I^{3\omega}_S}} \tag{2}$$

where d is the sample thickness, $I^{3\omega}$ and $I^{3\omega}_S$ are the THG intensities of the material studied and silica ($I^{3\omega}$= $I^{3\omega}_{[sample+substrate]}$-$I^{3\omega}_{[substrate]}$), respectively, and the coherence length of silica is given by

$$L_{c,S} = \frac{\lambda_\omega}{6(n_{3\omega} - n_\omega)}. \tag{3}$$

3. Computational Methods

3.1. Calculation of Microscopic Optical Properties

The calculations of the microscopic optical properties were performed with the GAMESS US package [32].

The linear polarizability (α), first hyperpolarizability (β) and second hyperpolarizability (γ) tensor components, used in the oriented gas model to calculate the macroscopic nonlinear optical properties, were computed within DFT and with the MP2 method.

The DFT calculations were performed with the the GGA functional BLYP [33, 34], the correlation-corrected functionals, LYP [34] and PW91C[35] (Hartree-Fock (HF) exchange; GGA correlation), the hybrid functionals B3LYP [36], X3LYP [37] and BHHLYP [38] and with the long-range corrected version of the BLYP functional (LC-BLYP), where the amount of HF exchange increases continuously as a function of electron-electron separation distance [39]. We used the 6-311G** basis set for iodine, and 6-311++G** for the lighter atoms. The basis sets were obtained from the EMSL Basis Set Exchange Library [40, 41]. The tensors α, β and γ were evaluated by finite field (FF) differentiation using an electric field step, $f = 0.001$ a.u..

The microscopic unit considered was the asymmetric unit, consisting of a cation-anion pair plus a water molecule with their relative positions and

geometries as in the crystal (since the optimized structure of this molecular cluster was very different from that obtained with the X-ray diffraction study, as the structure optimization performed in vacuum does not take in consideration the crystalline environment). The optical properties of the molecule 6-aminoquinoline, as well as those of the 6-aminoquinolinium cation, were also computed. The geometries of the molecule and of the cation were optimized with X3LYP/6-311G** calculations. The initial geometry of the neutral molecule, prior to the geometry optimization, was obtained by removing the proton bonded to the quinoline N atom. These optical properties have been evaluated in the gas phase.

As an alternative to the use of the local field corrections, we described the polarizing effects of the crystalline environment using electrostatic potential (ESP)-derived charges placed in atomic positions of the neighbors of the asymmetric unit. The ESP charges were calculated with the module CHELPG of the ORCA electronic structure package version 2.9.1 [42]. The program CHELPG calculates the atomic charges according to the CHELPG method (CHarges from Electrostatic Potentials using a Grid based method) developed by Breneman and Wiberg [43]. The calculation of the ESP charges was performed at the Hartree-Fock level with the 6-311G** basis set for iodine, and 6-311++G** for the lighter atoms. The microscopic optical properties where then calculated for the asymmetric unit surrounded by ESP charges of the atoms within a range of 11Å, totalling 750 charges (only complete molecular fragments were included). The atomic positions of the ESP charges were selected with the UCSF Chimera software package version 1.8 [44].

3.2. Calculation of Macroscopic Optical Properties

In most organic molecular crystals one can assume that the intermolecular interactions are much weaker than the intramolecular chemical bonds. In this situation, the oriented gas model [13] can be used to relate the macroscopic susceptibilities with the molecular hyperpolarizabilities. In this model, the molecular hyperpolarizabilities are assumed to be additive and the crystalline susceptibilities are obtained by performing a tensor sum of the microscopic hyperpolarizabilities of the molecules that constitute the unit cell. The susceptibility components depend on the crystal symmetry, the precise orientation of the molecule with respect to the crystal axes and the conformation of the molecule. For the second order susceptibility the following expression

applies:

$$d_{IJK}(-\omega;\omega_1,\omega_2) = \frac{1}{2}\chi^{(2)}_{IJK}(-\omega;\omega_1,\omega_2)$$
$$= \frac{N}{V} f_I(\omega) f_J(\omega_1) f_K(\omega_2) \frac{1}{N_g} \sum_s \sum_{ijk} \cos\theta^{(s)}_{Ii} \cos\theta^{(s)}_{Jj} \cos\theta^{(s)}_{Kk} \qquad (4)$$
$$\times \beta^{(s)}_{ijk}(-\omega;\omega_1,\omega_2)$$

where I, J, K are the crystal axes, N_g is the number of equivalent positions in the unit cell of volume V that has N molecules, $f_I(\omega)$ are local field factors appropriate for the crystal axis I, and the cosine product terms represent the rotation from the molecular reference frame onto the crystal frame. The equivalent positions are labeled by the index s. The local field factors, are essentially a correction for the difference between an applied field that would be felt by the molecule in vacuum and the local field inside the material. A generalization of this expression applies for the relation between the third-order optical susceptibility $\chi^{(3)}_{IJKL}(-\omega;\omega_1,\omega_2,\omega_3)$ and the molecular third-order polarizability, $\gamma_{ijkl}(-\omega;\omega_1,\omega_2,\omega_3)$, with one more local field factor for the frequency ω_3, $f_L(\omega_3)$. In most of the studies published so far, the oriented gas model is used with the Lorenz-Lorentz (L-L) local field correction [45] but there is evidence that the L-L local field factors may introduce errors of 50 % or more [46]. Wortmann and Bishop (W-B)[18] deduced new local field factors using an extension of the Onsager's reaction field model. These local field factors (W-B) had been used to estimate second- [47, 48] and third-order [49] macroscopic nonlinear optical properties, yielding better results than the L-L local field correction.

In this study, we calculated the second- and third-order macroscopic nonlinear optical properties of (**I**), using the oriented gas model with the Lorentz-Lorentz (L-L) [45] and the Wortmann and Bishop (W-B)[18] local field factors, using the values of the molecular optical properties obtained in the *ab initio* calculations.

The third-order susceptibility was also calculated by the summation of the third-order polarizabilities obtained in the calculations with the ESP charges describing the crystalline environment. In this kind of calculation the local field factors are set to 1 since we are summing effective third-order polarizabilities.

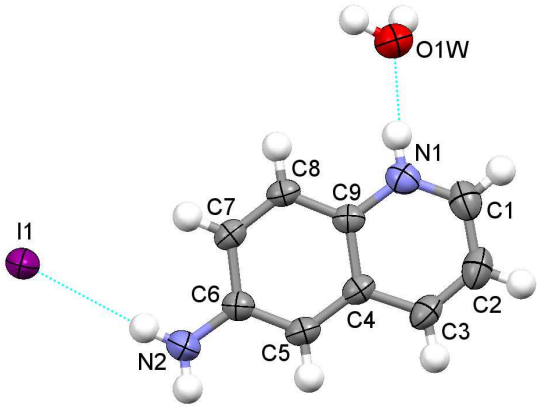

Figure 1: Asymmetric unit of 6-aminoquinolinium iodide monohydrate with thermal ellipsoids drawn at the 50% probability level (Mercury [50]).

4. Results and Discussion

4.1. Crystal Structure

The crystal structure of the title compound, (**I**) (Fig. 1), belongs to the orthorhombic system with the noncentrossymmetric and chiral space group $P2_12_12_1$. The asymmetric unit of (**I**) consists of one 6-aminoquinolinium cation with an iodide counter-ion and a water molecule. The cation is essentially planar with the ring atoms and the amino group having a RMS deviation of 0.0118 Å. The geometry of the quinolinium fragment is similar to that found in other aminoquinolinium salt structures [51, 52, 53]. The protonation of the quinoline N atom leads to an increase in the angle C-N-C [123.4(3)°] comparing with the same angle in quinoline [117.0(1)°] [54]. The C6-N2 bond to the amino nitrogen is short [1.357(4)Å], reflecting its π-character.

There are five conventional hydrogen bonds in this structure (see Table 2 and Fig. 2). The graph-set descriptors [55, 56] for basic first- and second-level sets, involving these hydrogen bonds, are presented in Table 3. It is evident the preponderance of finite graphs and this is consistent with the substantial involvement of the iodide ion and the water molecule, neither possessing special symmetry, in the hydrogen bonding. At the second level, we find two chains with descriptor $C_2^1(4)$. One is a *zigzag* chain along the *b* axis, with the cations linked to the anions via the amino group (hydrogen

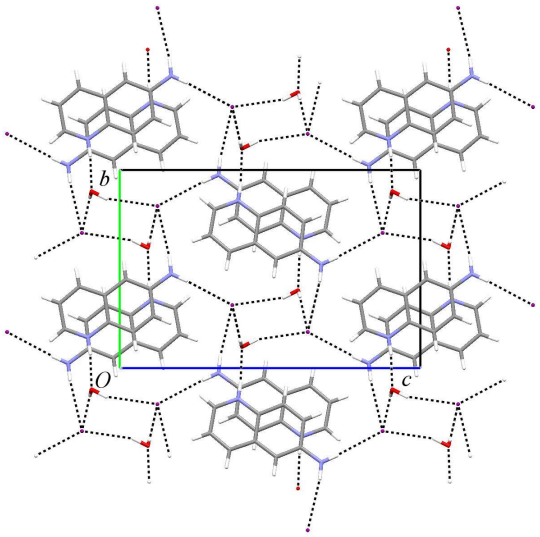

Figure 2: Packing diagram of (**I**) viewed down the a axis, with the hydrogen bonds depicted as dashed lines.

bonds labeled b and c in Table 2). The other is an helical chain propagating along the a axis, with the water molecules linked to the anions (hydrogen bonds labeled d and e in Table 2).

The crystal structure is also stabilized by π-π interactions between neighboring cations with antiparallel orientation, forming stacks along [100]. There are two different π-π interactions between pyridine and benzene rings with ring centroid separations of 3.696(2) and 3.726(2)Å. There is also one π-π interaction between adjacent benzene rings, with a distance between ring centroids of 3.715(2)Å.

Supplementary data have been deposited at the Cambridge Crystallographic Data Centre (CCDC No. 871464). This data can be obtained free of charge upon request from The Cambridge Crystallographic Data Centre via `www.ccdc.cam.ac.uk/data_request/cif`.

4.2. Absorption and Fluorescence Spectra

UV-visible absorption spectra of the title compound were recorded in the range 190-750 nm, in water solutions with concentrations ranging from 1.3×10^{-5} to 2.5×10^{-4} mol/L. The normalized UV-visible absorption spectrum for $c = 3.1 \times 10^{-5}$ mol/L is shown in Fig. 3. The spectrum has 3 intense bands

Table 2: Hydrogen-bonding geometry (Å,°) of (**I**).

D-H$\cdots A$	D-H	H$\cdots A$	$D\cdots A$	D-H$\cdots A$
a N1-H1A$\cdots$O1W^{i}	0.86	1.89	2.745(3)	173.7
b N2-H2A$\cdots$I1^{ii}	0.86	2.85	3.695(3)	165.8
c N2-H2B$\cdots$I1^{iii}	0.86	2.85	3.683(3)	164.8
d O1W-H1W$\cdots$I1^{iv}	0.86	2.80	3.620(3)	158.5
e O1W-H2W$\cdots$I1^{v}	0.86	2.76	3.584(2)	161.7

symmetry codes $i: -x+2, y+1/2, -z+1/2; ii: -x+3/2, -y+1, z+1/2;$ $iii: x+1/2, -y+3/2, -z+1; iv: x+1, y, z; v: x+1/2, -y+3/2, -z.$

Table 3: Basic first- and second-level graph-set descriptors involving the hydrogen bonds of Table 2.

	a	b	c	d	e
a	D	$D_2^2(10)$	$D_2^2(10)$	$D_2^2(4)$	$D_2^2(4)$
b		D	$C_2^1(4)$	$D_2^1(3)$	$D_2^1(3)$
c			D	$D_2^1(3)$	$D_2^1(3)$
d				D	$C_2^1(4)$
e					D

with maxima at 198, 222 and 256 nm and a broader band with λ_{max}=377 nm. The cutoff wavelength is around 460 nm. The spectrum of the unsubstituted quinolinium cation consists of two main features, an intense band centered at 240 nm involving $\pi - \pi^*$ transitions and a low-intensity feature centered at 320 nm, presumably involving $n - \pi^*$ excitations, however in a study of derivatives of quinolinium iodide it was shown that the presence of strong electron donor or acceptor groups cause a splitting of the intense shorter wavelength band and a broadening of the low-intensity feature at longer wavelength [12]. In the present case, the amino substituent acts as a strong electron donor and may be responsible for the band splitting. The molar extinction coefficients ε (see Table 4) were calculated from the Beer-Lambert law using solutions with concentrations in the range 1.3×10^{-5} - 2.5×10^{-4} mol/L. We found no evidence for aggregation at these concentrations, as we obtained good linear plots ($r \geq 0.998$) passing through the origin.

As we can see, the sample has some absorption at 355 nm. The value is small but can still have some effect on the THG response. In the calculations of the third-order susceptibility, presented in this study, we did not take this effect into account and we assumed it to be low.

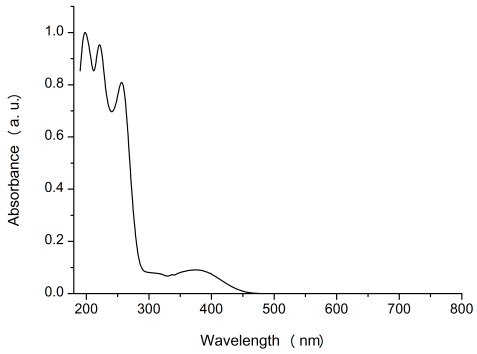

Figure 3: Normalized UV-visible absorption spectrum of the title compound ($c = 3.1\times10^{-5}$ mol/L in water solution)

Table 4: Absorption data for (**I**) in water solution.

λ_{max} [nm] (ε [M^{-1} cm^{-1}])			
198 (3.19×10^4)	222 (3.06×10^4)	256 (2.68×10^4)	377 (3.33×10^3)

The steady-state fluorescence emission spectrum (see Fig. 4), taken with excitation at 377 nm, presents one maximum at 558 nm. The spectroscopic singlet-state energy (E_S=2.6 eV) was obtained from the intersection of the normalized absorption and fluorescence spectra. The observed emission spectrum shows good mirror symmetry with the lowest-energy absorption band.

4.3. Nonlinear Optical Properties

4.3.1. Z-Scan

The nonlinear absorption of the title compound was investigated with "open-aperture" Z-scan measurements performed for water solutions with concentrations ranging from 0.5 to 2 mM. Within experimental accuracy, no two-photon absorption was observed for all concentrations studied.

4.3.2. SHG and THG Measurements

The effective second- and third-order nonlinear optical susceptibilities, $\chi^{(2)}$ and $\chi^{(3)}$ respectively, were measured with the Maker fringes technique. The absolute value of $\chi^{(2)}$ was evaluated by comparing the SHG signal with

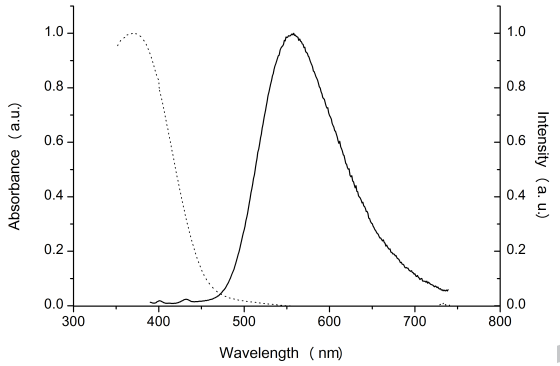

Figure 4: Normalized absorption (dotted curve) and fluorescence (solid curve) spectra in the range 350-750 nm.

that from quartz (0.6 pm/V) [57]. The SHG results were very weak: $(1.04 \pm 0.06) \times 10^{-3}$pm/V for the s-s polarization and $(1.44 \pm 0.41) \times 10^{-3}$pm/V for the p-p polarization.

For the evaluation of the absolute value of $\chi^{(3)}$, the reference material used was fused silica (2×10^{-22} m^2/V^2) [58]. The value of third-order NLO susceptibility $\chi^{(3)}$ for (**I**) at λ=1064nm has been estimated to be $(4.51 \pm 0.96) \times 10^{-21}$m^2/V^2, for the s-s polarization, and $(4.94 \pm 0.60) \times 10^{-21}$m^2/V^2, for the p-p polarization.

We present in Fig. 5 an example of characteristic experimental curves for a THG Maker fringes measurement with thin film of compound (**I**). The irregularity of the Maker fringes signal is due to the inhomogeneity of the thin film of compound (**I**).

4.3.3. Calculated Microscopic NLO properties

The α_{ij}, β_{ijk} and γ_{ijkl} tensor components were calculated according to the methods described in 3.1 for the 6-aminoquinolinium cation, for the 6-aminoquinoline molecule, for the asymmetric unit and for the asymmetric unit surrounded by 750 ESP-derived charges. In all calculations the molecular axis are the same as the crystalline: $x = a$; $y = b$; $z = c$. The charge transfer interaction occurs mainly in the yz molecular plane and the tensor components in the z direction are dominant for the β_{ijk} and γ_{ijkl} tensors. In Table 5 we present the calculated values of the first and second hyperpolarizabilities along the z direction, for the different levels of theory used.

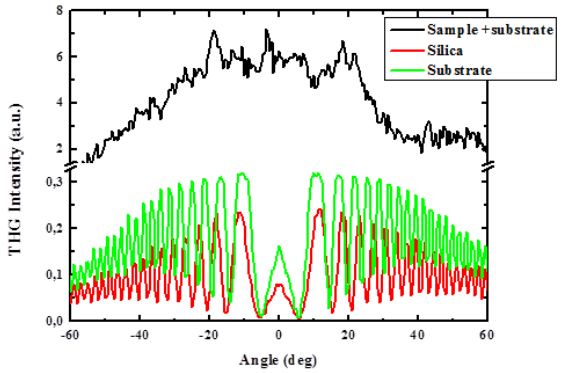

Figure 5: An example of THG Maker fringes signal as function of the angle of incidence for a thin film of compound (**I**), observed by using a Nd-YAG laser of 1064 nm

The values calculated for the neutral molecule and for the cation show a reasonable consistency for all methods used. However, for the asymmetric unit calculations, it is evident the very large discrepancy between the values obtained with the hybrid functionals (B3LYP, X3LYP and BHHLYP), the GGA functional BLYP, and all the other calculations. Such enormous differences disappear when the ESP-derived charges are included in the calculation.

It is well-known that DFT overestimates molecular charge-transfer properties namely, nonlinear optical properties. This has been investigated thoroughly for conjugated molecular chains [14, 15, 16]. This deficiency is associated with a poor treatment of the electron exchange.

There are some approaches to correct this problem and one of those is the use of a high percentage of HF-exchange [14, 16]. This problem is also addressed by the long-range corrected (LC) functionals. In the LC method, the long-range orbital-orbital interactions are explicitly included in the exchange functional by combining DFT exchange with the HF exchange integral [39]. Contrasting with the density partitioning schemes such as B3LYP or X3LYP, the proportion of nonlocal HF contribution in LC varies according to the range of the interaction. This is done by separating the two-electron operator into short-range and long-range parts by using the standard error function. In this way the ratio of the nonlocal HF part to the local DFT part becomes larger for greater distances.

The performance of the functionals with exact HF exchange (LYP and PW91C) and of the long-range corrected functional (LC-BLYP) seems to

Table 5: Theoretical values of the first and second hyperpolarizabilities (a.u.) along the z direction for the 6-aminoquinoline molecule (6AQ), the 6-aminoquinolinium cation ($6AQ^+$), the asymmetric unit ($6AQ^+I^-w$) and the asymmetric unit surrounded by 750 ESP-derived charges within a radius of 11Å ($6AQ^+I^-w$ ESP). The calculations were performed for different levels of theory with the 6-311G** basis set for iodine and 6-311++G** for the lighter atoms.

	6AQ		$6AQ^+$		$6AQ^+I^-w$		$6AQ^+I^-w$ ESP	
	β_{zzz}	γ_{zzzz}	β_{zzz}	γ_{zzzz}	β_{zzz}	γ_{zzzz}	β_{zzz}	γ_{zzzz}
BLYP	-767.7	77998	-1315.7	47082	3.65×10^5	-2.95×10^8	-3408.6	527745
B3LYP	-686.9	63560	-1311.8	57647	-1.86×10^4	-1.71×10^7	-2648.6	199427
X3LYP	-687.5	64108	-1312.6	58937	-2.68×10^4	-2.62×10^7	-2626.3	193753
BHHLYP	-607.8	54414	-1262.7	65043	-1.81×10^4	-1.63×10^7	-2241.5	137312
LC-BLYP	-615.8	51580	-1182.5	63128	-4209.2	592401	-2134.8	124302
LYP	-507.7	41727	-1160.6	66908	-3075.0	216169	-1856.2	111242
PW91C	-499.1	38611	-1142.0	64266	-2962.4	200136	-1805.2	109721
MP2	-697.2	63851	-1332.1	62825	-4132.8	348764	-2386.1	136133

be more reasonable, comparing with the hybrid functionals and the GGA functional. The inclusion of the ESP charges seems to remedy also this computational artifact related to the charge overdelocalization between the cation and the anion.

Looking at the values calculated for the asymmetric unit surrounded by ESP-derived charges, it is evident a decrease of the hyperpolarizabilities with the increase of the percentage of HF exchange (BLYP: 0%; B3LYP and X3LYP: 20%; BHHLYP: 50%; LYP and PW91C: 100%).

Evans *et al.*[10] demonstrated the utilization of acid/base proton transfer to enhance the hyperpolarizabilities of the chromophores and our calculations show also an increase of the component β_{zzz} upon protonation. If we consider the interaction between the cations and anions there is a further increase in the molecular NLO properties.

4.3.4. Calculated Macroscopic NLO properties

By the 222-D_2 symmetry and the Kleinman symmetry there is only one non-vanishing independent component of the second-order polarizability tensor for the title compound , *i.e.*, d_{XYZ}, so this point group is not very favorable for SHG applications.

For a material belonging to any orthorhombic group the tensor $\chi^{(3)}$ have 21 independent nonzero elements and far from resonance, under the assumption that there is no energy dissipation through the nonlinear process, Kleinman symmetry can be used to reduce the number of independent components to 6: $\chi^{(3)}_{iiii}$ $(i = x, y, z)$ and $\chi^{(3)}_{iijj}$ $(i = x, j = y, z;\ i = y, j = z)$. The average

Table 6: Theoretical values of the second and third-order susceptibilities estimated with the oriented gas model with L-L and W-B local-field factors, using microscopic optical properties calculated for several levels of theory. The chromophoric unit considered was the asymmetric unit.

		$\chi^{(2)}$ (pm/V))	$\chi^{(3)}$ (10^{-21}m^2/V^2)
LYP	L-L	1.9	30.3
	W-B	1.0	6.6
PW91C	L-L	1.7	26.5
	W-B	0.9	5.9
LC-BLYP	L-L	3.3	121.9
	W-B	1.6	17.1
MP2	L-L	3.9	88.3
	W-B	1.8	13.7
Experimental	s-s	$(1.04 \pm 0.06) \times 10^{-3}$	(4.51 ± 0.96)
	p-p	$(1.44 \pm 0.41) \times 10^{-3}$	(4.94 ± 0.60)

third-order susceptibility is then given by

$$\chi^{(3)} = \frac{1}{5}(\chi^{(3)}_{xxxx} + \chi^{(3)}_{yyyy} + \chi^{(3)}_{zzzz} + 2\chi^{(3)}_{xxyy} + 2\chi^{(3)}_{xxzz} + 2\chi^{(3)}_{yyzz}) \quad (5)$$

Using the calculated microscopic optical properties, the second- and third-order susceptibilities of (**I**) were estimated using the oriented gas model with the Lorentz-Lorentz (L-L) [45] and the Wortmann and Bishop (W-B)[18] local field factors. Regarding the physical nature of the thin films, it was assumed that the material is microcrystalline with the same symmetry as the original single crystals. The presence of SHG signal suggests this. For the calculation of the effective third-order susceptibility, this assumption is not critical since an amorphous material can generate a THG signal. The results of these calculations are presented in Table 6.

The comparison of the two local-field corrections indicate that the calculations using the Lorenz-Lorentz factors yield generally higher susceptibilities, and the difference is quite large for the calculated $\chi^{(3)}$ values. The calculations predict a small value for the second-order susceptibility, but not with the same order of magnitude of the experimental values. This may be explained by the presence of non-crystalline material in the thin film. Nevertheless, since the experimental SHG results are very weak it is difficult to draw any conclusions for the calculations from the comparison of the calculated and experimental $\chi^{(2)}$ values.

Table 7: Theoretical values of the third-order susceptibilities (10^{-21}m^2/V^2) estimated using the effective third-order polarizability tensor calculated for the asymmetric unit surrounded by 750 ESP-derived charges within a radius of 11Å.

Method	BLYP	B3LYP	X3LYP	BHHLYP	LC-BLYP	LYP	PW91C	MP2	Exp. s-s/p-p
$\chi^{(3)}$	3.8	1.8	1.8	1.4	1.3	1.1	1.0	1.5	4.51 ± 0.96/ 4.94 ± 0.60

The theoretical values of the third-order susceptibility $\chi^{(3)}$ were also estimated using the effective third-order polarizability tensor components γ_{ijkl}^{eff} obtained by the inclusion of 750 ESP-derived charges within a radius of 11Å of the asymmetric unit, to model the effect of the crystalline environment. These results are presented in Table 7.

Regarding the second-order nonlinearities, it is interesting to note a relation between the crystal structure and the low SHG results. Zyss and Oudar [59] deduced relations between the macroscopic and molecular second-order optical nonlinearities for the case of a two-dimensional molecular unit. For the point group 222,

$$b_{XYZ} = \sin 2\Phi \cos\alpha(\beta_{yxx} - \beta_{yyy} \sin^2 \alpha) - \beta_{xyy} \cos 2\Phi \sin 2\alpha \qquad (6)$$

where α is the angle between the molecular plane and the macroscopic axis Y (crystallographic b axis) and Φ is the angle between the molecular plane and the macroscopic X (crystallographic a axis). See figures 1 and 2 on reference [59] for the definition of the macroscopic crystalline and microscopic molecular axis. According to eq. 6, when Φ=90 ° and α=0 ° the value of b_{XYZ} is zero. In our structure, the cations are almost perfectly parallel to the plane (100), making an angle of 89.45(5)° with the a axis and 0.03(5)° with the b axis. The iodide anions closer to the cations are near the plane of the cations and the charge transfer between the ions can be considered as being approximately two-dimensional. We can thus conclude that, although the molecules have a robust optical response, the packing of the chromophoric units in this crystal structure is very unfavorable for SHG. Even a perfect crystallized material would yield very low $\chi^{(2)}$ values.

Concerning the third-order susceptibility, the calculations predict the correct order of magnitude with the W-B local field factors. The use of the γ tensor values calculated with the functionals B3LYP, X3LYP, BHHLYP and BLYP, in the absence of ESP-derived charges, would lead to third-order susceptibilities two to three orders of magnitude larger than the experimental ones and we don't present this results as they are not physically meaning-

ful. Using the summation of the effective third-order polarizability tensor components γ_{ijkl}^{eff} calculated for the asymmetric unit surrounded by the ESP-derived charges, all the third-order susceptibilities are of the same order of magnitude of the experimental.

5. Conclusions

A new semi-organic compound, 6-aminoquinolinium iodide monohydrate, was synthesized and structurally characterized by single crystal X-ray diffraction. The linear and nonlinear optical properties of this compound were studied with UV-vis absorption and fluorescence spectroscopy, "open-aperture" Z-scan technique and Maker fringes techniques (SHG and THG). The microscopic β and γ tensor components were calculated with the DFT and MP2 methods. The macroscopic susceptibilities of second- and third order were estimated with the oriented gas model in its most general formulation using two different local-field corrections. The calculations using the W-B local-field factors were able to reproduce the correct order of magnitude of the experimental third-order susceptibilities. The third-order susceptibilities obtained by the summation of the effective third-order polarizability tensors calculated for the asymmetric unit surrounded by the ESP-derived charges are also of the same order of magnitude as the experimental.

6. Acknowledgements

This work was supported by the Fundo Europeu de Desenvolvimento Regional QREN-Compete through the projects PTDC/FIS/103587/2008, PEst-C/FIS/UI0036/2011 and PTDC/AAC-CLI/098308/2008 Fundação para a Ciência e a Tecnologia (FCT). PSPS acknowledges the scholarship SFRH/BPD /84173/2012 and CTA acknowledges the scholarship SFRH/BD/48269/2008 of FCT.

References

[1] D. S. Chemla, J. Zyss (Eds.), Nonlinear Optical Properties of Organic Molecules and Crystals, volume 1, Academic Press, Orlando, FL, 1987.

[2] J. Zyss (Ed.), Molecular Nonlinear Optics. Materials, Physics, and Devices, Academic Press, Boston, MA, 1994.

[3] S. R. Marder, J. W. Perry, W. P. Schaefer, Science 245 (1989) 626.

[4] P. J. Lacroix, R. Clément, K. Nakatani, J. Zyss, I. Ledoux, Science 263 (1994) 658.

[5] P. Günter, C. Bosshard, K. Sutter, H. Arend, G. Chapuis, R. J. Twieg, D. Dobrowolski, Appl. Phys. Lett. 50 (1987) 486.

[6] Z. Kotler, R. Hierle, J. Zyss, J. Opt. Soc. Am. B 9 (1992) 534.

[7] N. Horicuhi, F. Lefaucheux, A. Ibanez, D. Josse, J. Zyss, J. Opt. Soc. Am. B 19 (2002) 1830.

[8] S. Manivannan, S. Dhanuskodi, K. Kirschbaum, S. K. Tiwari, Cryst. Growth Des. 5 (2005) 1463.

[9] W. Bi, N. Louvain, N. Mercier, J. Luc, I. Rau, F. Kajzar, B. Sahraoui, Adv. Mater. 20 (2008) 1013.

[10] C. C. Evans, M. Bagieu-Beucher, R. Masse, J.-F. Nicoud, Chem. Mater. 10 (1998) 847.

[11] K. Bouchouit, E. E. Bendeif, H. El-Ouazzani, S. Dahaoui, C. Lecomte, N. Benali-cherif, B. Sahraoui, Chem. Phys. 375 (2010) 1.

[12] A. Zelichenok, V. Burtman, N. Zenou, S. Yitzchaik, S. D. Bella, G. Meshulam, Z. Kotler, J. Phys. Chem. B 103 (1999) 8702.

[13] D. S. Chemla, J. L. Oudar, J. Jerphagnon, Phys. Rev. B 12 (1975) 4534.

[14] B. Champagne, E. Perpète, S. J. A. van Gisbergen, E. J. Baerends, J. G. Snijders, C. Soubra-Ghaoui, K. A. Robins, B. Kirtman, J. Chem. Phys 109 (1998) 10489.

[15] S. J. A. van Gisbergen, P. R. T. Schipper, O. V. Gritsenko, E. J. Baerends, J. G. Snijders, B. Champagne, B. Kirtman, Phys. Rev. Lett. 83 (1999) 694.

[16] B. Champagne, E. A. Perpète, D. Jacquemin, S. J. A. van Gisbergen, E. J. Baerends, C. Soubra-Ghaoui, K. A. Robins, B. Kirtman, J. Phys. Chem. A 104 (2000) 4755.

[17] K. Y. Suponitsky, Y. Liao, A. E. Masunov, J. Phys. Chem. A 113 (2009) 10994.

[18] R. Wortmann, D. M. Bishop, J. Chem. Phys. 108 (1998) 1001.

[19] L. Onsager, J. Am. Chem. Soc. 58 (1936) 1486.

[20] K. Y. Suponitsky, A. E. Masunov, J. Chem. Phys. 139 (2013) 094310.

[21] H. Hu, D. A. Fishman, A. O. Gerasov, O. V. Przhonska, S. Webster, L. A. Padilha, D. Peceli, M. Shandura, Y. P. Kovtun, A. D. Kachkovski, I. H. Nayyar, A. E. Masunov, P. Tongwa, T. V. Timofeeva, D. J. Hagan, E. W. V. Stryland, J. Phys. Chem. Lett. 3 (2012) 1222.

[22] S. Draguta, M. S. Fonari, A. E. Masunov, J. Zazueta, S. Sullivan, M. Y. Antipin, T. V. Timofeeva, CrystEngComm 15 (2013) 094310.

[23] Bruker, SMART and SAINT, Bruker AXS Inc., Madison, Wisconsin,USA, 2003.

[24] G. M. Sheldrick, SADABS, University of Göttingen, Germany, 1996.

[25] G. M. Sheldrick, Acta Cryst., Sect. A 64 (2008) 112.

[26] M. Sheik-Bahae, A. A. Said, T. H. Wei, D. J. Hagan, E. W. V. Stryland, IEEE J. Quantum Electron. 26 (1990) 760.

[27] R. Zaleśny, O. Loboda, K. Iliopoulos, G. Chatzikyriakos, S. Couris, G. Rotas, N. Tagmatarchis, A. Avramopoulos, M. G. Papadopoulos, Phys. Chem. Chem. Phys. 12 (2010) 373.

[28] P. D. Maker, R. W. Terhune, M. Nisenoff, C. M. Savage, Phys. Rev. Lett. 8 (1961) 21.

[29] G. J. Lee, S. W. Cha, S. J. Jeon, S. I. Jin, J. Korean Phys. Soc. 39 (2001) 912.

[30] R. A. Myers, N. Mukherjee, S. R. J. Brueck, Opt. Lett. 16 (1991) 1732.

[31] K. Kubodera, H. Kobayashi, Mol. Cryst. Liq. Cryst. 182 (1990) 103.

[32] M. W. Schmidt, K. K. Baldridge, J. A. Boatz, S. T. Elbert, M. S. Gordon, J. H. Jensen, S. Koseki, N. Matsunaga, K. A. Nguyen, S. Su, T. L. Windus, M. Dupuis, J. A. Montgomery, J. Comput. Chem. 14 (1993) 1347.

[33] A. D. Becke, Phys. Rev. A 38 (1988) 3098.

[34] C. Lee, W. Yang, R. G. Parr, Phys. Rev. B 37 (1988) 785.

[35] J. P. Perdew, Y. Wang, Phys. Rev. B 45 (1992) 13244.

[36] A. D. Becke, J. Chem. Phys. 98 (1993) 5648.

[37] X. Xu, W. A. G. III, PNAS 101 (2004) 2673.

[38] A. D. Becke, J. Chem. Phys. 98 (1993) 1372.

[39] H. Iikura, T. Tsuneda, T. Yanai, K. Hirao, J. Chem. Phys. 115 (2001) 3540.

[40] D. Feller, J. Comp. Chem. 17 (1996) 1571.

[41] K. L. Schuchardt, B. T. Didier, T. Elsethagen, L. Sun, V. Gurumoorthi, J. Chase, J. Li, T. L. Windus, J. Chem. Inf. Model. 47 (2007) 1045.

[42] F. Neese, WIREs Comput. Mol. Sci. 2 (2012) 73.

[43] C. M. Breneman, K. B. Wiberg, J. Comput. Chem. 11 (1990) 361.

[44] E. F. Pettersen, T. D. Goddard, C. C. Huang, G. S. Couch, D. M. Greenblatt, E. C. Meng, T. E. Ferrin, J. Comput. Chem. 25 (2004) 1605.

[45] J. Schwinger, L. L. D. Jr, K. A. Milton, W. Y. Tsai, Molecular Nonlinear Optics. Materials, Physics, and Devices, Perseus Books, Cambridge, MA, 1998.

[46] P. T. van Duijnen, A. H. de Vries, M. Swart, F. Grozema, J. Chem. Phys. 117 (2002) 8442.

[47] P. S. P. Silva, C. Cardoso, M. R. Silva, J. A. Paixao, A. M. Beja, M. H. Garcia, N. Lopes, J. Phys. Chem. A 114 (2010) 2607.

[48] S. R. Domingos, P. S. P. Silva, W. J. Buma, M. H. Garcia, N. C. Lopes, J. A. Paixao, M. R. Silva, S. Woutersen, J. Chem. Phys. 136 (2012) 134501.

[49] Y. Luo, P. Norman, P. Macak, H. Ågren, Phys. Rev. B 61 (2000) 3060.

[50] C. F. Macrae, P. R. Edgington, P. McCabe, E. Pidcock, G. P. Shields, R. Taylor, M. Towler, J. van de Streek, J. Appl. Cryst. 39 (2006) 453.

[51] G. Smith, U. D. Wermuth, J. M. White, Acta Cryst., Sect. C 60 (2004) o575.

[52] J. Oueslati, A. Oueslati, C. B. Nasr, F. Lefebvre, Solid State Sci. 8 (2006) 1067.

[53] G. Smith, U. D. Wermuth, J. M. White, Acta Cryst., Sect. C 64 (2008) o180.

[54] J. E. Davies, A. D. Bond, Acta Cryst., Sect. E 57 (2001) o947.

[55] M. C. Etter, Acc. Chem. Res. 23 (1990) 120.

[56] J. Bernstein, R. E. Davis, L. Shimoni, N. L. Chang, Angew. Chem. Int. Ed. Engl. 34 (1995) 1555.

[57] C. Bosshard, U. Gubler, P. Kaatz, W. Mazerant, U. Meier, Phys. Rev. B 61 (2000) 10688.

[58] U. Gubler, C. Bosshard, Phys. Rev. B 61 (2000) 10702.

[59] J. Zyss, J. L. Oudar, Phys. Rev. A 26 (1982) 2028.

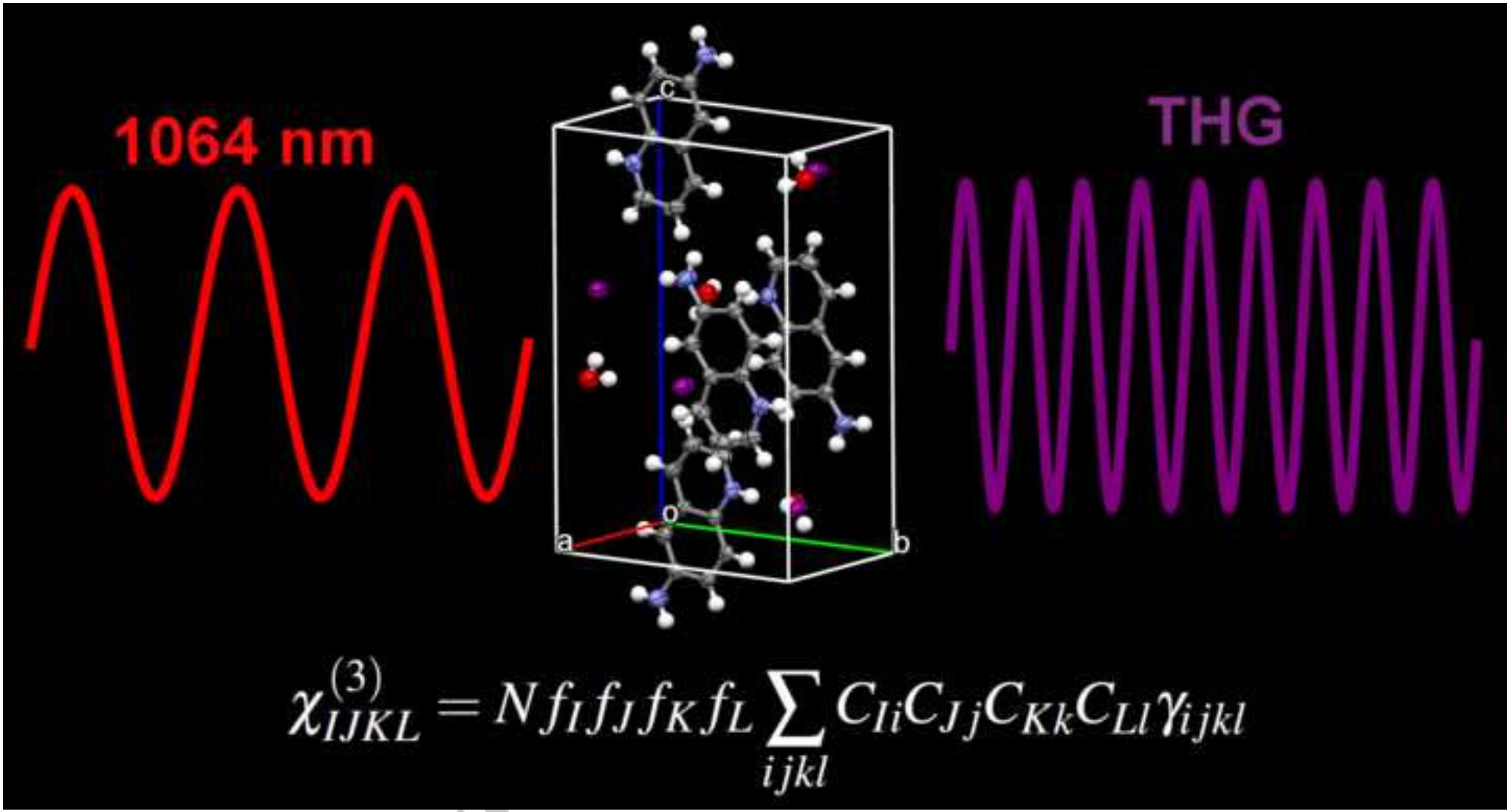

Highlights:

- Synthesis and structure of 6-aminoquinolinium iodide monohydrate is reported
- UV-vis absorption and fluorescence spectra are reported
- SHG and THG signals measured with the Maker fringes technique
- Hyperpolarizabilities calculated with the DFT and MP2 methods
- Behaviour of hybrid functionals corrected with ESP charges